Microstructure Dependent Properties of Polypropylene-Clay Nanocomposites

Y. Fan, J. Lou, D. M. Shinozaki

Department of Mechanical and Materials Engineering, The University of Western Ontario, London, Ontario, Canada N6A 5B8

Received 8 June 2006; accepted 11 July 2006
DOI 10.1002/app.25144
Published online in Wiley InterScience (www.interscience.wiley.com).

ABSTRACT: The mechanical properties of melt processed polypropylene-montmorillonite nanocomposites were studied as a function of clay content. The measurement of tensile properties at room temperature and dynamic mechanical properties over a wide temperature range reveal a decrease in modulus and tensile strength of the composite with increasing clay content. The origins of this anomalous result were examined in detail using X-ray diffraction and differential scanning calorimeter, which averaged the microstructure over reasonable specimen volumes. Micromechanical models could be used to adequately describe the composite properties, provided appropriate properties for the matrix and particle were used. The matrix properties were found to affect the average properties significantly. © 2006 Wiley Periodicals, Inc. J Appl Polym Sci 103: 204–210, 2007

Key words: modulus; polypropylene (PP); crystallization; composites; clay

INTRODUCTION

The use of nanometer sized clay in thermoplastics is the subject of a number of recent publications. The underlying practical reason for the interest is in the reported improvements in properties, which arise when the clay is added. Of particular interest are the mechanical properties of such nanocomposites based on a polypropylene (PP) matrix.[1–4] Compatibility is achieved by chemically modifying the clay to produce a hydrophobic surface[5] and using a maleated form of polypropylene (PP-*g*-MA).[6,7] Melt processing of these materials involves the mixing of the components: PP, maleated PP, and clay to achieve uniform dispersion of the nanometer-sized reinforcement phase. Previously, it has been reported that the mechanical properties of the composite could be optimized by using a clay to PP-*g*-MA ratio of approximately (1 : 3).[8–10] The present study attempts to examine the separate effects of the two components used in the fabrication of melt mixed PP nanocomposites, PP-*g*-MA, and clay, on the mechanical properties of the melt mixed nanocomposite. Standard micromechanical models are used to reveal the influence of the matrix and particle properties on the composite behavior. X-ray diffraction and thermal analysis were used suitably to average the appropriate microstructural parameters.

Correspondence to: D. M. Shinozaki (shinozaki@uwo.ca).
Contract grant sponsor: NSERC.

EXPERIMENTAL

Materials

An extrusion grade low molecular weight PP (Atofina 3825) was used as the base matrix material. The compatibilizer was Epolene G-3003 (Eastman Chemical, Eastport, TN), a maleated PP with 0.8 wt % maleic anhydride (PP-*g*-MA). This was selected after considering the reported tensile properties for a variety of commercially available maleated polypropylenes.[11] This had a moderate molecular weight (M_n = 27,200, M_w = 52,000). The montmorillonite clay was obtained from Southern Clay Products (Gonzales, TX) (Cloisite15A®) with a high degree of hydrophobicity. It is a natural montmorillonite modified with a quaternary ammonium salt (125 meq/mg clay). This was received in powder form with a wide distribution of agglomerated particle sizes less than approximately 13 μm. A preliminary comparison of the mechanical properties of nanocomposites showed that the use of Cloisite 15A® resulted in better properties than Cloisite 20A, which has a lower modifier concentration.

Processing

The components were dried in an air oven at 80°C for 24 h. The clay and PP-*g*-MA were then premixed in a mixer (Model D-51-T, C. W. Brabender Instruments) at room temperature. The ratio of maleated PP to clay was fixed at 3 : 1 (wt). The proportions of materials used for the two composites and their respective matrices are shown in Table I, where the

TABLE I
Sample Composition

	Cloisite 15A® (wt %)	PP-*g*-MA (wt %)
1 wt % clay	1	3
5 wt % clay	5	15
Matrix : 3 wt % MA	0	3
Matrix : 15 wt % MA	0	15

1 wt % clay sample contains 3 wt % maleated compatibilizer and the 5 wt % clay contains 15 wt %.

The PP was added to the mixer after the other materials. The melt mixing was run at 185°C at 100 rpm for 5 min, using the high shear blades. The mixed material was air cooled and cut into small irregular pieces. The amounts are consistent with those reported in the literature to produce well dispersed nanocomposites.[12]

After mixing, the material was transfer molded into a solid plaque ($50 \times 20 \times 0.8$ mm^3), using a hydraulic press with heated plates. Care was taken to eliminate voids in the final sample. The melt flow patterns in the mold were similar to those found in an injection molded part.

The plaques and the as-mixed melt were examined using X-ray diffraction on Philips X-ray diffractometer. The experiments used Cu Kα radiation with a wavelength of 1.542 Å monochromatized with a transmission nickel filter. Tube voltage and current were set to 40 kV and 20 mA, respectively.

Thermal properties of the various samples were measured using a Perkin–Elmer DSC7 differential scanning calorimeter (DSC). Standard calibrations for specimen temperature and heat of fusion were regularly run with indium and zinc. The measurement of crystallinity using DSC provided values, which were averaged over reasonable volumes of specimen. Temperature dependent dynamic mechanical properties (storage modulus and loss factor) were measured using a polymer laboratories dynamic mechanical thermal analyzer. A frequency of 1 Hz with small amplitude was set for the measurements, and the instrument was calibrated before each test. The measurements were made by step-wise scanning over a temperature range of $40°C < T < 150°C$.

Tensile tests at a nominal strain rate of 8×10^{-4} sec^{-1} were performed on a Sintech QT150 at room temperature using an MTS 1250 N load cell. For improved sensitivity and testing flexibility, the load–displacement data were acquired using a separate data acquisition system connected externally.

RESULTS AND DISCUSSION

Dispersion of clay

The differences in X-ray diffractometer scans for the nanocomposites can be seen in Figure 1 compared to the base PP and pure clay. The trace for PP (A), is characteristic of unoriented material consisting principally of monoclinic α phase. The pure clay (compacted as-received powder) shows two low angle peaks (D); the major one for a periodicity of approximately 3.1 nm, close to the 3.15 nm spacing reported by the supplier, Southern Clay Products. A secondary peak is seen at about 1.23 nm. This has been described as evidence for a second distinct clay tactoid population with a different periodic spacing,[13] since it does not correspond to a second order diffraction peak.

With melt mixing of the 5 wt % clay sample, the scan C shows that the major low angle peak shifts to a smaller angle, indicating an increase in average spacing to about 3.39 nm. The secondary peak is too small to measure its position precisely, but the average spacing increases to approximately 1.3 nm. The peak sizes diminish with decreasing clay content, as expected.

An examination of the expected differences in peak position and peak size suggests other microstructural effects. For smaller clay content (1 wt %) (B), the principal peak shifts even further than the 5 wt % clay sample, to larger spacing (3.75 nm). The secondary peak position cannot be resolved since the intensity is too low. The obvious implication is that the intercalation process is inversely related to the clay content. This observation has been explained in terms of the inability of the long chain maleated

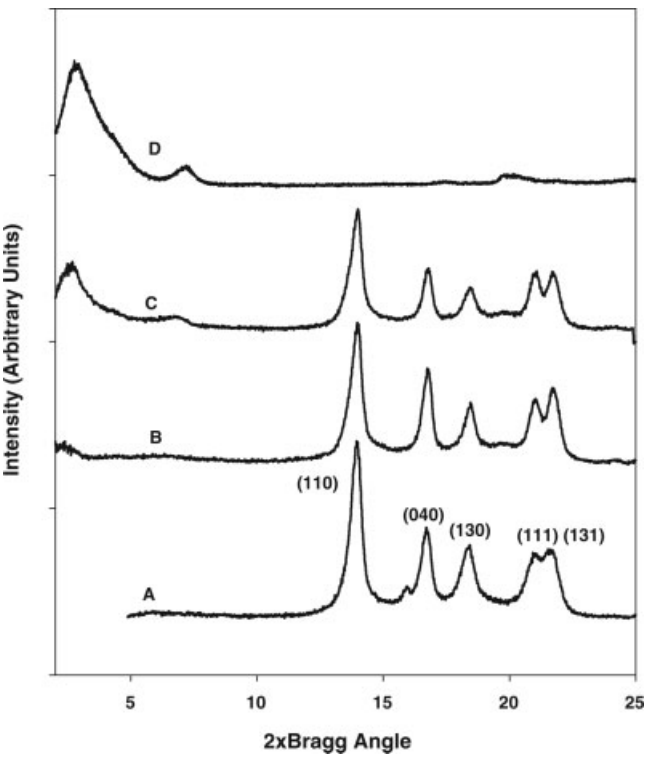

Figure 1 X-ray diffractometer scans for: (A) polypropylene, (B) 1 wt % clay nanocomposite, (C) 5 wt % clay nanocomposite, and (D) compacted Cloisite 15A® powder.

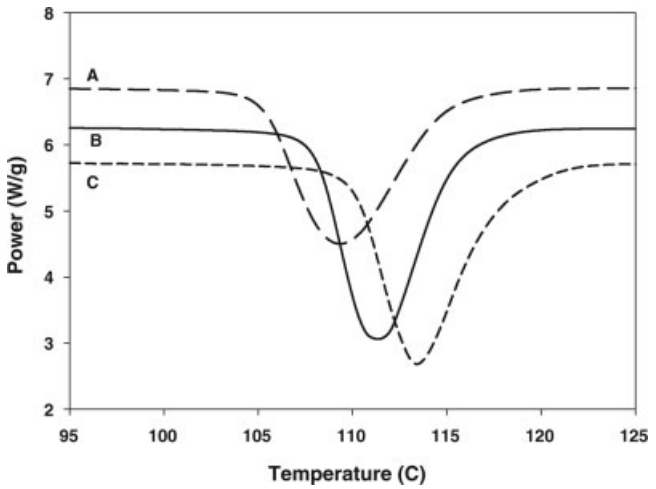

Figure 2 DSC crystallization exotherms cooled at 20°C/min for: (A) polypropylene, (B) matrix consisting of PP mixed with 3 wt % PP-*g*-MA, and (C) 1 wt % clay nanocomposite.

PP (M_W = 52,000) to diffuse effectively in the high volume fraction clay material.[11,13] However, the physical interpretation of the Bragg diffraction peak also has a bearing on the analysis. The peak is the integrated sum of diffraction from many tactoids, the shift in position of the peak maximum can be a result of all tactoids increasing in spacing uniformly, or the fraction of tactoids with smaller spacing may increase in spacing disproportionately.

The 5 wt % clay peak area scales appropriately with the pure clay sample if the physical density of the compressed clay powder used for these samples is considered then the presence of residual voids in the sample is a result of incomplete compaction. However, the 1 wt % clay peak area is only 10% of the corresponding peak in the 5 wt % clay sample, suggesting a larger extent of exfoliation in the 1 wt % clay sample compared to the 5 wt %. Thus both the peak position shift and the changes in peak area are consistent with the conclusion that the 1 wt % clay sample is more completely exfoliated than the sample with higher clay concentration. This conclusion is also consistent with other reported work.[13]

For the different specimens, the PP diffraction peaks in Figure 1 do not shift in Bragg angle with intercalation and mixing but show an intensity loss at the higher clay content. This is due to the decrease in mass of crystalline phase contributing to the diffraction peak. The change in amount of crystalline material is likely due, partly decreasing PP mass (as clay is added) and, to the changes in crystallinity due to the presence of the compatiblized clay particle surfaces.

Crystallization of the matrix

In terms of the processing parameters, differences in crystallinity of the matrix can affect the nanocomposite properties. The crystallization process involves molecular reorganization during solidification. Both the chemical composition of the matrix and the distribution and average spacing of the clay particles are expected to influence the crystallization.

The comparison of cooling curves for the nanocomposite, the matrix (consisting of PP and PP-*g*-MA) and the basic PP are shown in Figures 2 and 3. The samples were cooled from the melt at a rate of 20°C/min in the DSC. These show that the addition of clay increases the temperatures of both the onset of crystallization (T_o) and the peak (T_p) for the 1 wt % and the 5 wt % clay samples compared to the matrix phase in each case. This is expected since the clay has been modified to compatibilize the surface, and the interface between the clay and the matrix would have a reduced surface energy, enhancing the tendency to crystallize.

However, if the thermal properties of the two samples are compared with each other, the increase in clay from 1 to 5 wt % reduces the crystallization temperature. This is because of the reduction in crystallization temperatures in the matrix phase as a result of the increase in maleated fraction in the matrix molecule.

From the viewpoint of melt processing, the dependence of the crystallization behavior on the cooling rate through the solidification temperature is of some significance. The crystallization onset and peak temperatures are plotted as functions of the cooling rate in Figures 4 and 5. An increase in cooling rate systematically reduces both, suggesting the clay enhances the crystallization process.

The crystallinities for the different nanocomposites were also estimated from the heats of fusion measured in the DSC scans (Figs. 6 and 7). The heat of

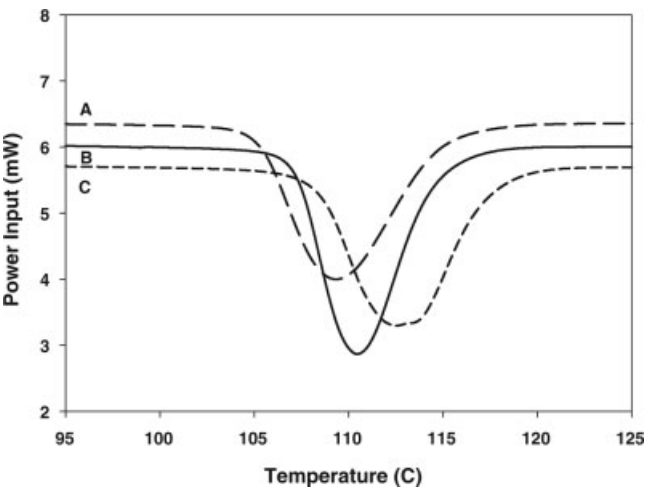

Figure 3 DSC crystallization exotherms cooled at 20°C/min for: (A) polypropylene, (B) matrix consisting of PP mixed with 15 wt % PP-*g*-MA, and (C) 5 wt % clay nanocomposite.

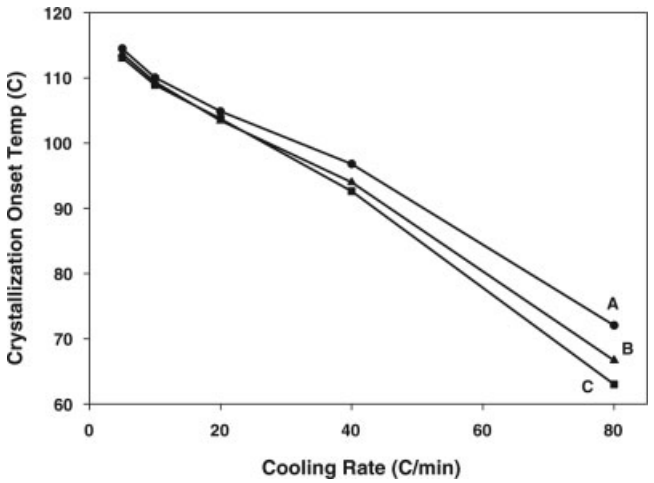

Figure 4 Crystallization peak temperature as a function of rate of cooling from the melt: (A) 1 wt % clay nanocomposite, (B) polypropylene, and (C) 5 wt % clay nanocomposite.

fusion for α (monoclinic) phase of PP has been reported to be 150 J/g.[13] The crystallinity decreases in all samples with increasing cooling rate, as expected for a nucleation and growth process in which the rates of cooling are sufficient to suppress the overall crystallization rates. For these nonisothermal cooling processes, the molecular mobility decreases with decreasing temperature, and as a result the growth rate is reduced.

It is interesting to note that the sample with 5 wt % clay has lower crystallinity than the sample with 1 wt % clay. In addition, the temperatures for the onset and the peak of crystallization show this apparent anomalous behavior. However this is consistent with the conclusion made from the X-ray diffraction results earlier that the lower clay content results in a greater degree of exfoliation in the composite.[8] The greater degree of exfoliation in the 1 wt % sample produces a greater total surface area of clay in the melt, and the resultant enhancement in crystallinity and crystallization rate.

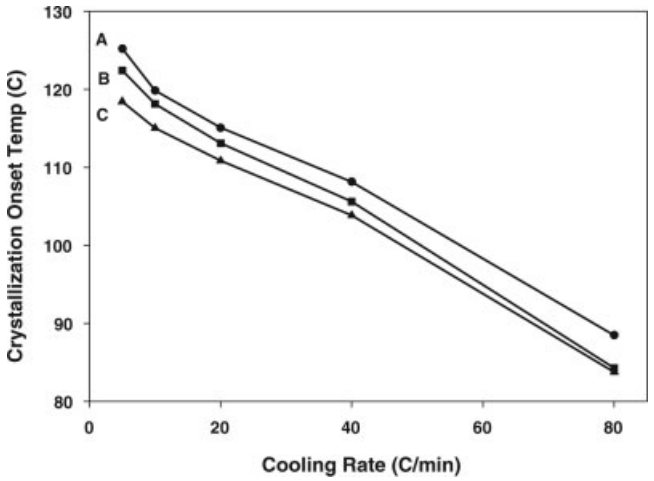

Figure 5 Crystallization onset temperature as a function of cooling rate from the melt: (A) 1 wt % clay nanocomposite, (B) 5 wt % clay nanocomposite, and (C) polypropylene.

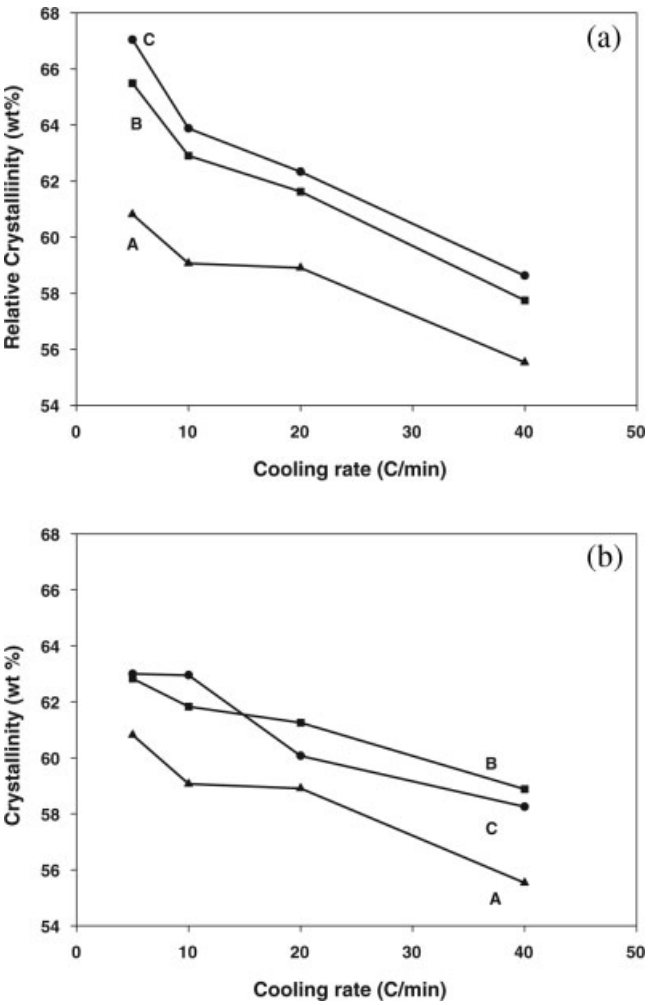

Figure 6 (a) Relative crystallinity (wt %) calculated from DSC crystallization exotherms plotted as a function of cooling rate from the melt: (A) polypropylene, (B) matrix consisting of PP mixed with 3 wt % PP-*g*-MA, and (C) 1 wt % clay nanocomposite. (b) Relative crystallinity calculated from DSC crystallization exotherms plotted as a function of cooling rate from the melt: (A) polypropylene, (B) matrix consisting of PP mixed with 15 wt % PP-*g*-MA, and (C) 5 wt % clay nanocomposite.

Storage modulus

The moduli of the matrices (PP with 3 wt % and 15 wt % PP-*g*-MA, respectively) were plotted as function of temperature in Figure 7, compared to the PP base material. The sample with 3 wt % PP-*g*-MA, which is the matrix for the 1 wt % clay nanocomposite, has a higher measured modulus than sample with 15 wt % PP-*g*-MA, which is the matrix for the 5 wt % clay nanocom-

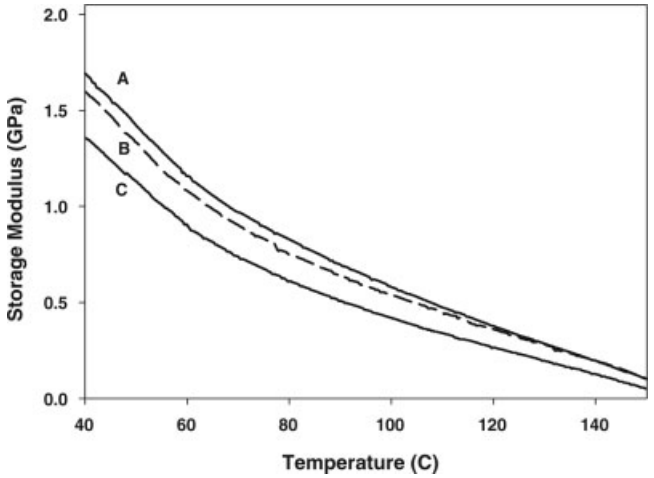

Figure 7 Temperature dependence of matrix storage modulus for: (A) PP, (B) matrix consisting of PP mixed with 3 wt % PP-*g*-MA, and (C) matrix consisting of PP mixed with 15 wt % PP-*g*-MA.

posite. This is due, at least in part, to the higher crystalline content shown in Figure 6. It is significant to note that the PP itself has a higher modulus than the matrix materials, even though the crystallinity of the unmodified PP is lower.

The temperature dependent storage moduli measured for clay reinforced matrices are shown in Figure 8. The 1 wt % clay nanocomposite has a significantly higher modulus than does the 5 wt %, apparently due at least in part to the higher modulus of the matrix. The weakening effect resulting from the addition of maleated PP is compensated by the strengthening effect due to the clay. However, the 1 wt % clay still has a higher modulus than the 5 wt % clay nanocomposite, consistent with the higher degree of exfoliation at the lower clay content.

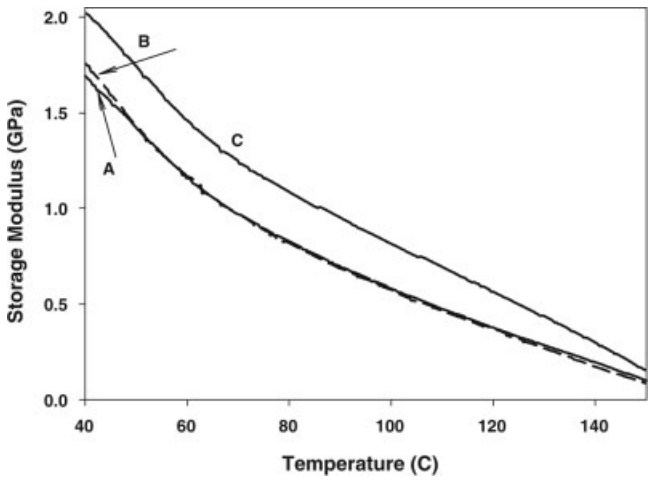

Figure 8 Comparison of the measured temperature dependence of the storage modulus for: (A) PP, (B) 5 wt % clay nanocomposite, and (C) 1 wt % clay nanocomposite.

A cross comparison between the nanocomposites with their respective matrices in Figures 7 and 8 shows that the introduction of the clay increases the modulus significantly in each case. The compatibilizer (PP-*g*-MA) clearly acts to reduce the modulus.

It is finally interesting to examine more carefully the temperature dependence of the storage modulus. The 1 wt % clay nanocomposite generally shows a greater reduction in modulus at high temperatures (near 140°C) compared to the 5 wt % sample. The relative effect is seen in Figure 9, in which the nanocomposite moduli are normalized with respect to their respective matrix moduli. The relatively inferior reinforcing effect of the 5 wt % clay nanocomposite is clearly seen at lower temperatures. The clay increases the modulus by a factor of 1.2–1.4. In contrast the 1 wt % nanocomposite shows that the addition of this smaller amount of clay increases the modulus by a factor of 1.2–1.7. The 1 wt % clay sample therefore reinforces the material more efficiently than 5 wt %, probably because of the increased degree of exfoliation. It is interesting to note that the effectiveness of reinforcement increases sharply above 140°C for the 5 wt %, becoming similar to the 1 wt % clay nanocomposite at these higher temperatures. This is likely due to crystallization occurring in the matrix at these temperatures. This is not observed in the 1 wt % sample because of the relatively high crystallinity in the matrix (Fig. 6).

Micromechanical effects

The matrix and reinforcement effects seen in the storage modulus can be examined further using micromechanical models. The simplest models (Voigt and

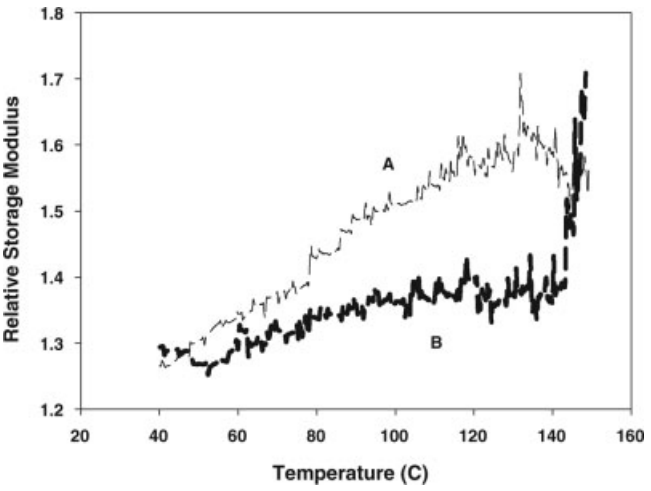

Figure 9 Relative temperature dependent modulus for: (A) 1 wt % clay nanocomposite and (B) 5 wt % clay nanocomposite. (Normalized with respect to the relevant matrix phase in each case.)

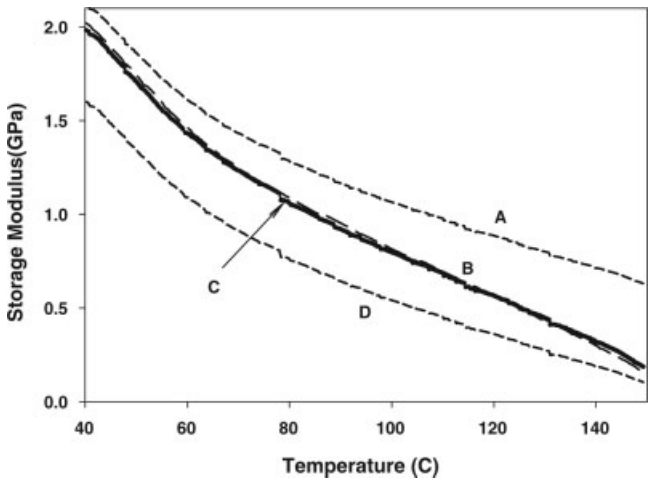

Figure 10 Comparison of experimental temperature dependent storage modulus with micromechanical models for 1 wt % clay nanocomposite: (A) Voigt, (B) Halpin-Tsai for oriented clay ($K = 1$), (C) experimental, and (D) Reuss.

Reuss) provide upper and lower bounds to the composite modulus:

$$\text{Voigt}: E_c = (1 - V_f)E_m + V_f E_f \tag{1}$$

$$\text{Reuss}: \frac{1}{E_c} = \frac{V_f}{E_f} + \frac{1 - V_f}{E_m} \tag{2}$$

where V_f is the volume fraction of the reinforcing phase, and E_c, E_f, and E_m are the moduli of the composite, the reinforcing phase, and the matrix, respectively.

The Halpin-Tsai model incorporates further details of the reinforcing phase shape to obtain a more accurate predicted modulus.[14] The model parameters include factors, which are dependent on the platelet shape and orientation found in clay nanocomposites:

$$E_c = \frac{E_m}{K}\frac{1 + \xi\eta V_f}{1 - \eta V_f} \tag{3}$$

$$\eta = \frac{E_f/E_m - 1}{E_f/E_m + \xi} \tag{4}$$

$$\xi = 2\frac{w}{t} + 40V_f^{10} \tag{5}$$

The average platelet shape is described by the width to thickness ratio w/t, which has been reported by the manufacturer to be 150 for fully exfoliated clay. K describes the average orientation of the platelets[15] ($K = 1$ for fully oriented platelets and $K = 3$ for the fully randomized platelets).

These models can be used for estimating composite storage modulus, provided the temperature is well away from the glass transition (T_g), which for PP is in the range between -5 and -20°C. To examine the appropriateness of these kinds of standard models for nanocomposites, the parameters were measured independently.

The temperature dependent modulus for the matrix (E_m) was obtained experimentally over a range of temperatures well away from T_g. Over the same temperature range, the modulus of the clay was expected to be constant at $E_f = 170$ GPa.

It was necessary to estimate the true volume fraction of the reinforcing clay phase since the as-received clay consisted of montmorillonite (the reinforcing phase) and an organic interlayer, which is relatively soft. For as-received Cloisite 15A®, the weight loss on ignition was reported by the manufacturer to be 43 wt %. The volume fraction of the clay was calculated to be 0.31% and 1.57% for the 1 and 5 wt % samples used in the present article. In terms of modeling, the interlayer, the organic modifier, and the matrix were assumed to have similar properties.

The effectiveness of the mechanical reinforcement effect of clay in these nanocomposites can be understood by comparing the experimentally measured temperature dependent storage moduli for the 1 and 5 wt % clay specimens. The lower volume fraction modulus is shown in Figure 10 compared to the various standard analytical models. The Halpin-Tsai model (curve B for $K = 1$) fits the measured data (C) very well over the entire temperature range. At low temperatures the nanocomposite tends to approach the Voigt (parallel coupled) model (A) while at high temperatures, where the matrix softens considerably, it shifts to more closely agree with the Reuss (series coupled) model (D). This is expected from the func-

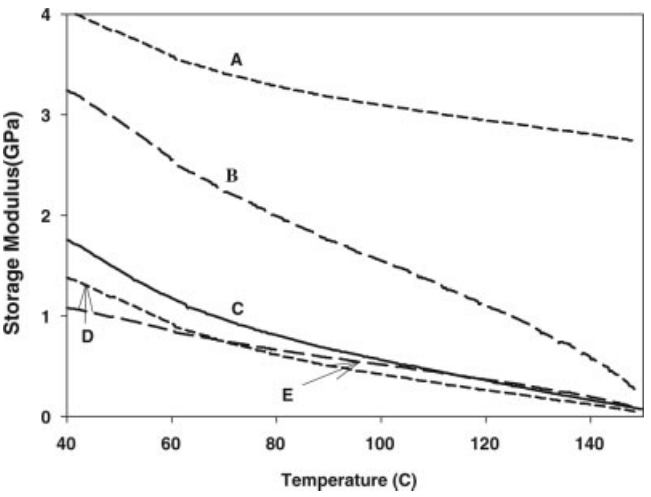

Figure 11 Comparison of experimental temperature dependent storage moduli for 5% nanocomposite: (A) Voigt, (B) Halpin-Tsai for oriented clay ($K = 1$), (C) experimental, (D) Reuss, and (E) Halpin-Tsai for unoriented clay ($K = 3$).

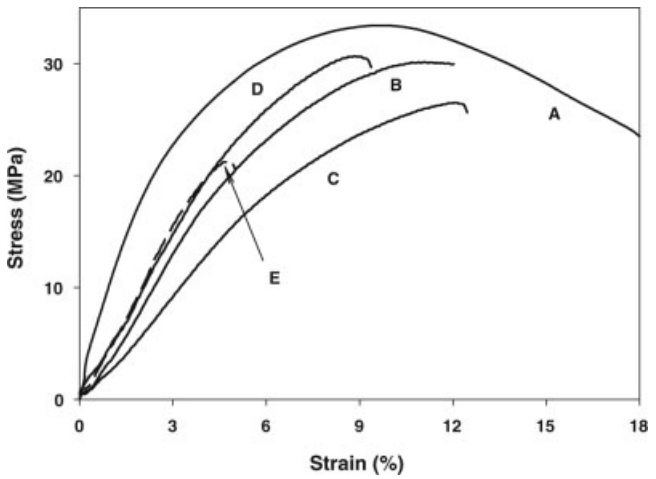

Figure 12 Comparison of tensile stress-strain curves for: (A) PP, (B) matrix consisting of PP mixed with 3 wt % PP-*g*-MA, (C) matrix consisting of PP mixed with 15 wt % PP-*g*-MA, (D) 1 wt % clay nanocomposite, and (E) 5 wt % clay nanocomposite.

tional forms of the models. The modeling clearly points to clay platelets, which are highly oriented.

The 5 wt % clay modulus is shown in Figure 11. The experimentally determined storage modulus lies near the softer Reuss model (D) over the entire temperature range. It is distinctly lower than the Halpin Tsai prediction for oriented platelets (curve B for $K = 1$). The clay is, on average, less highly oriented than the 1 wt % clay sample seen in Figure 10. A qualitative explanation for this may lie in the increase in melt viscosity at the higher clay content, and with the lower tactoid aspect ratio found in nonexfoliated clay, which leads to a lower tendency to align in the flow field. It is also likely that the relatively low crystallinity in the 5 wt % samples is partially responsible for this effect.

The conclusion that the 1 wt % clay is highly oriented also supports the earlier suggestion that the X-ray diffraction results show that the 1 wt % sample is fully exfoliated. Highly aligned nonexfoliated tactoids should show a much stronger diffraction peak in Figure 1.

Tensile properties: Ductility

The effects of the various components in the nanocomposite on the tensile properties are consistent with the measured tensile properties shown in Figure 12. The full ductility of the PP is not shown on this scale, being typically greater than 500%. Addition of increasing amounts of maleated PP progressively reduces the tensile modulus and strength compared to the PP itself. In addition the ductility is reduced. The clay further reduces the ductility, although the modulus increases a small amount. The tensile fracture occurs before the specimen develops the characteristic stable neck seen in PP. It is clear that the maleated component and the clay itself accelerate the onset of the plastic instability, which precedes fracture in these materials. The necking and failure in PP develops in conjunction with micro-cavitation generated by the inhomogeneous plasticity in the microstructure. The maleated PP reduces the tensile strength of the material, allowing this kind of instability to develop more readily. The clay accentuates the heterogeneity of the plasticity, which also allows for local deformation instabilities to initiate at low applied stresses.

CONCLUSIONS

The storage modulus of the nanocomposite was found to be consistent with standard composite micromechanical models provided the appropriate properties of the matrix and the reinforcing particles were used. The microstructural parameters of interest were measured experimentally over reasonable specimen volumes using DSC and X-ray diffraction. The matrix properties were affected by the maleated PP, which reduced the ductility and storage modulus of the final nanocomposite and act to reduce the stiffening effect of the clay particles.

The assistance of B. Verhagen has been invaluable in completing this work.

References

1. Ma, J.; Qi, Z.; Hu, Y. J Appl Polym Sci 2001, 82, 3611.
2. Wang, Y.; Chen, F. B.; Li, Y. C.; Wu, K. C. Compos B 2004, 35, 11.
3. Ton-That, M. T.; Perrin-Sarazin, F.; Cole, K. C.; Bureau, M. N.; Denault, J. Polym Eng Sci 2004, 44, 1212.
4. Xu, W.; Liang, G.; Wang, W.; Tang, S.; He, P.; Pan, W. J Appl Polym Sci 2003, 88, 3225.
5. Leuteritz, A.; Pospiech, D.; Kretzschmar, B.; Willeke, M.; Jehnichen, D.; Jentzsch, U.; Grundke, K. Adv Eng Mater 2003, 5, 678.
6. Reichert, P.; Nitz, H.; Klinke, S.; Brandsch, R.; Thomann, R.; Mülhaupt, R. Macromol Mater Eng 2000, 275, 8.
7. Hasegawa, N.; Okamoto, H.; Kato, M.; Usuki, A. J Appl Polym Sci 2000, 78, 1918.
8. Kawasumi, M.; Hasegawa, N.; Kato, M.; Usuki, A.; Okada, A. Macromolecules 1997, 30, 6333.
9. Kato, M.; Usuki, A.; Okada, A. J Appl Polym Sci 1997, 66, 1781.
10. Wang, Y.; Chen, F.; Wu, K. J Appl Polym Sci 2004, 93, 100.
11. Svoboda, P.; Zeng, C.; Wang, H.; Lee, L.; Tomsko, D. J Appl Polym Sci 2002, 85, 1562.
12. Hasegawa, N.; Usuki, A. J Appl Polym Sci 2004, 93, 464.
13. Bond, E. B.; Spruiell, J. H.; Lin, J. S. J Polym Sci Part B: Polym Phys 1999, 37, 3050.
14. Halpin, J. C. Primer on Composite Materials; Technomic: Lancaster, PA, 1984.
15. Ulutan, S.; Gilbert, M. J Mater Sci 2000, 35, 2115.